Processing and Application of Ceramics 10 [2] (2016) 57–66
DOI: 10.2298/PAC1602057R

Carbonate apatite formation on novel multiphase $CaO\text{-}SiO_2\text{-}P_2O_5\text{-}MgO$ glass-ceramics in TRIS-HCl buffer

Lachezar Radev[1,*], Irena Michailova[2], Hristo Georgiev[3], Diana Zaimova[1]

[1]*Department of Fundamental Chemical Technology, University of Chemical Technology and Metallurgy, Sofia, Bulgaria*
[2]*Department of Silicate Technology, University of Chemical Technology and Metallurgy, Sofia, Bulgaria*
[3]*Department of Polymer Engineering, University of Chemical Technology and Metallurgy, Sofia, Bulgaria*

Received 2 April 2016; Received in revised form 24 May 2016; Accepted 31 May 2016

Abstract

The main purpose of the presented article is the preparation of novel glass-ceramics in $CaO\text{-}SiO_2\text{-}P_2O_5\text{-}MgO$ system and evaluation of carbonate apatite formation after soaking in TRIS-HCl buffer solution for 14 days. The investigated samples were prepared via sol-gel method and structure of the obtained samples was studied using XRD, FTIR, SEM, XPS and ICP-AES. XRD of the thermally treated samples showed that the presence of some crystalline phases is depended on the gel composition. FTIR revealed the existence of all characteristic bands for the observed crystalline phases. SEM monitored the presence of particles with different morphology. After soaking in TRIS-HCl solution, FTIR confirmed that carbonate apatite was formed on the soaked surface. The obtained data are in a good agreement with XPS analysis. The change of ions concentrations in TRIS-HCl buffer solution after immersion of the prepared glass-ceramics was recorded by ICP-AES measurements.

Keywords: *$CaO\text{-}SiO_2\text{-}P_2O_5\text{-}MgO$, glass-ceramics, TRIS buffer, carbonate apatite, in vitro bioactivity*

I. Introduction

It is known that the controlled bioactivity and degradation of glasses and glass-ceramics are needed to meet different clinical requirements. Previous studies have shown that the glass-ceramics in $CaO\text{-}SiO_2$ system possess good in vitro bioactivity [1]. Thus, $CaO\text{-}SiO_2$ system has been considered as the basis of many of the third generation tissue regeneration materials [2]. In 1980s, Nakajima *et al.* [3,4] developed magnesium doped $CaO\text{-}SiO_2$ diopside ($CaMgSi_2O_6$) ceramics. They used newly created biomaterial, because it was found that diopside possesses carbonate apatite (CO_3HA) formation ability in SBF solution and bonds to the bone when implanted in rabbits. Later Shyu and Wu [5] prepared $CaMgSi_2O_6/Ca_3(PO_4)_2$ composites after heat treatment of the gels at 990 °C for 1 h. Wu and co-workers [6,7] investigated akermanite ($Ca_2MgSi_2O_7$) and bredegite ($Ca_7MgSi_4O_{16}$) ceramics in $CaO\text{-}SiO_2\text{-}MgO$ system [6–9]. Their studies showed that these ceramics were degradable and revealed CO_3HA formation in SBF solution. In addition, the ionic products from them could stimulate osteoblast proliferation and differentiation. In another article Ma *et al.* [10] found that the incorporation of Mg promotes the crystallization of $Ca_2MgSi_2O_7$ and cristobalite (SiO_2), inducing the formation of wollastonite ($CaSiO_3$)/$Ca_2MgSi_2O_7$ based glass-ceramics. They also concluded that the incorporation of 10 mol.% MgO does not suppress *in vitro* bioactivity of the prepared samples. Bernardo *et al.* [11] fabricated $Ca_2MgSi_2O_7$ ceramics in the presence of silicone resins, used as silica source, filled with micro- and nano-sized CaO and MgO particles. Yoganand *et al.* [12] synthesized glass-ceramics in $CaO\text{-}MgO\text{-}SiO_2$ system via plasma-sintering method and observed the presence of $CaMgSi_2O_6$ and depicted that the synthesized sample showed the CO_3HA formation on the soaked surface in SBF solution. Hafezi-Ardakani *et al.* [13] synthesized pure nano-crystalline merwinite ($Ca_3Mg(SiO_4)_2$) by sol-gel method after thermal treatment of the powder at 1300 °C. On the basis of the *in vitro* bioactivity essay, the authors concluded that the prepared sample acts as a bioactive material: after the first day of soaking, apatite layer can be formed on its surface. Bala-

*Corresponding author: tel: +35 92 816 3280, fax: +35 92 868 5488, e-mail: *l_radev@abv.bg*

murugan *et al.* [14] synthesized bioglasses in the SiO_2-CaO-MgO-P_2O_5 system and observed that after thermal treatment at 1100 °C two crystalline phases can be detected – $(Ca,Mg)_3(PO_4)_2$ and forsterite (Mg_2SiO_4). On the basis of the *in vitro* test in SBF, they concluded that on the surface of the synthesized sample after 21 days of soaking, apatite crystalline phases were deposited. In an interesting article Tulyaganov *et al.* [15] synthesized glass-ceramics in CaO-MgO-SiO_2 system with addition of B_2O_3, P_2O_5, Na_2O and CaF_2. After thermal treatment of all compositions at 1400 °C for 1 h, XRD proved that highly dense and crystalline samples composed mainly of $CaMgSi_2O_6$ and wollastonite ($CaSiO_3$) with small amounts of $Ca_2MgSi_2O_7$ and residual glassy phase was observed. In the recent years Tulyaganov and co-workers [16] published the experimental investigation of a glass based on CaO-MgO-P_2O_5-Na_2O-CaF_2 system as a potential material for biomedical applications. They concluded that CO_3HA was formed at their surface after *in vitro* bioactivity test in SBF. On the other hand, *in vivo* animal studies revealed low inflammatory infiltrate with the surrounding tissue.

In the present work we faced two basic problems: *i*) to synthesize novel glass-ceramics in CaO-SiO_2-P_2O_5-MgO system with different (Ca+Mg)/(P+Si) molar ratio, and *ii*) to study the changes occurring at the surface of the glass-ceramics in TRIS-HCl solution. TRIS-HCl solution was used because of some previous studies on bioactive glass reactivity [17], as well as it does not contain any foreign ions, and is an excellent medium in order to analyze surface products on the prepared glass-ceramics.

II. Experimental work

2.1. Materials and methods

Two different CaO-SiO_2-P_2O_5-MgO materials were synthesized by multistage sol-gel method. In the first step SiO_2 sol was prepared from tetraethoxysilane (TEOS) by stirring with solvent (mixture of C_2H_5OH and H_2O) and a catalyst (a small amount of HCl) in a volume ratio TEOS : C_2H_5OH : H_2O : HCl = 1 : 1 : 1 : 0.01. After approximately 1 h and the formation of transparent solution, the magnesium salt ($Mg(NO_3)_2 \times 6H_2O$) dissolved in water was mixed with prehydrolysed TEOS under stirring for 14 h. In the second step calcium phosphate (CP) solution was prepared by mixing of $Ca(OH)_2$ and H_3PO_4 at pH = 10–11. The calcium phosphate mixture was added dropwise into the modified silica sol under intensive stirring. The prepared mixed sol was stirred for 24 h, gelled at 120 °C for 12 h and thermally treated at 1200 °C for 2 h in a tubular furnace. Chemical composition of the obtained gels and glass-ceramics is given in Table 1.

2.2. Corrosion test in TRIS-HCl buffer

The dissolution test of the obtained glass-ceramics was carried out in TRIS-HCl buffer. Briefly, the corresponding amount of TRIS powder ((hydrohymethyl) amino methane ($(CH_2OH)_3CNH_2$), necessary to obtain 1 M solution, was dissolved in water, and the pH was adjusted to ~7.4 with 2 M HCl. The desired amount of the glass-ceramic powder (0.5 g) was dissolved in a beaker with 50 cm^3 of the as prepared TRIS-HCl solution in a static condition at 36.6 °C. After 14 days of reaction in TRIS-HCl, the bulk glass-ceramic samples were washed with water and dried in an oven at 70 °C for 4 h.

2.3. Characterization techniques

The structure and in vitro bioactivity of the synthesized glass-ceramics were monitored by X-ray diffraction (XRD), Fourier transform infrared (FTIR) spectroscopy and scanning electron microscopy (SEM). XRD was collected within 2θ range from 10 to 80° with a constant step of 0.04° and counting time of 1 s/step on Brucker D8 Advance diffractometer with Cu$K\alpha$ radiation and SolX detector. FTIR transmission spectra were recorded by a Brucker Tensor 27 Spectrometer with scanner velocity 10 kHz. KBr pellets were prepared by mixing of ~1 mg of the sample with 300 mg KBr. Transmission spectra were recorded using MCT detector with 64 scans and 1 cm^{-1} resolution. The scanning electron microscope (SEM, Hitachi, TM3000) at an operating voltage of 15 kV was used to study the morphology of the thermally treated samples and for the apatite deposited on the surface of bioactive glass-ceramics, after soaking in TRIS-HCl buffer solution.

X-ray photoelectron spectroscopy (XPS) measurements were carried out with monochromatic Al Kα radiation using VG ESCALAB II electron spectrometer with energy of 1486.6 eV. The composition and chemical surrounding of the deposited films were investigated on the basis of the areas and binding energies of C1s, Ca2p, P2p, and Si2p photoelectron peaks.

The ions concentrations of Ca, P and Si after soaking in TRIS-HCl buffer for 7 days were recorded by inductively coupled plasma atomic emission spectroscopy (ICP-AES) using IRIS 1000, Thermoelemental, USA.

III. Results and discussion

3.1. Samples before soaking in TRIS-HCl solution

XRD patterns of the C-1 and C-2 samples, sintered at 1200 °C for 2 h, are presented in Fig. 1. In

Table 1. Chemical composition of the prepared glass-ceramics

Samples	Composition of the gels [wt.%]				Ca+Mg/Si+P molar ratio
	CaO	SiO_2	P_2O_5	MgO	
C-1	38	29	31	2	1.00
C-2	55	20	22	3	2.18

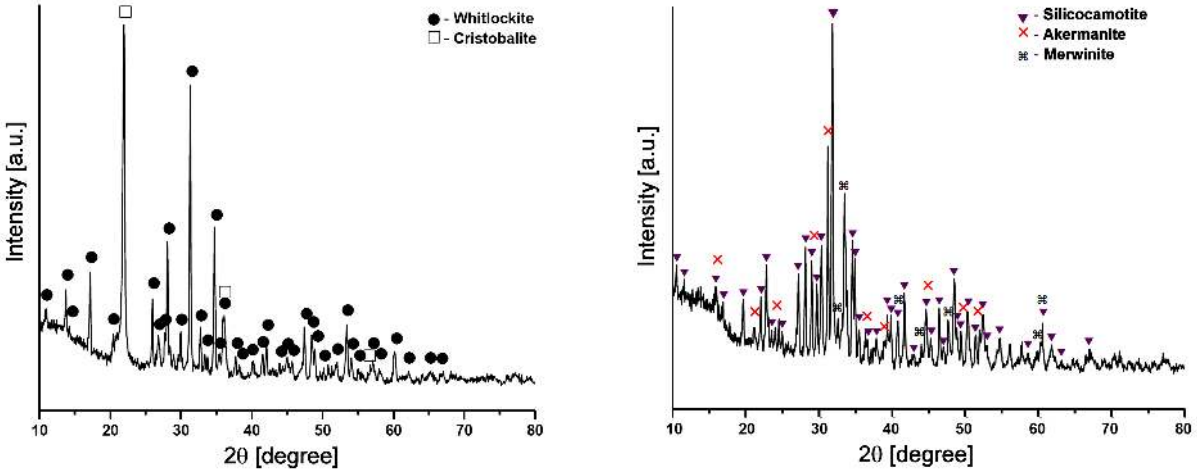

Figure 1. XRD of the C-1 (a) and C-2 (b) glass-ceramics after thermal treatment at 1200 °C for 2 hours

accordance with our preliminary results [18], in the magnesia-free glass-ceramics some crystalline phases can be detected, such as: calcium phosphate silicate ($Ca_{15}(PO_4)_2(SiO_4)_6$), wollastonite ($CaSiO_3$) and pseudowollastonite ($Ca_3(Si_3O_9)$). In this context, Ma *et al.* [10,19,20] also reported that in the CaO-P_2O_5-SiO_2 glass-ceramics, XRD proved the presence of $CaSiO_3$ and $Ca_3(Si_3O_9)$. As can be seen from Fig. 1 the glass-ceramics containing magnesia has the following crystalline phases: *i*) whitlockite, $(Ca,Mg)_3(PO_4)_2$ (PDF card 70-2064), and cristobalite, SiO_2 (PDF card 85-0512) in the sample C-1 and ii) silicocarnotite, $Ca_5(PO_4)_2SiO_4$ (PDF card 40-0293), $Ca_2MgSi_2O_7$ (PDF card 79-2425) and $Ca_3MgSi_2O_8$ (PDF card 74-0382) in the sample C-2. In accordance with some preliminary results [10,19,20], the incorporation of magnesia in the CaO-SiO_2-P_2O_5 gels induces the formation of cristobalite. On the other hand, Watts *et al.* [21], concluded that in the case of SiO_2-P_2O_5-CaO-MgO-Na_2O bioactive glasses, the part of magnesia acts as network intermediate and exists in Si-O-Si network as MgO_4 tetrahedral units. It was also observed [22] that akermanite contains tetrahedral MgO_4 units.

Figure 2 shows FTIR spectra of the samples, thermally treated at 1200 °C for 2 h. The presented FTIR spectra of the samples sintered at 1200 °C showed the characteristic bands for the sol-gel glasses and glass-ceramics. According to the previous investigations [23], three optical vibration modes of Si-O groups can be observed. The band posited at 1085 (1056) cm^{-1} corresponds to the Si-O-Si symmetric stretching vibration, and the bands around 477 cm^{-1} may be defined as Si-O-Si vibration. The band at ~490 cm^{-1} could be assigned to the vibration of Si-O-Mg bond [24]. In addition, the shoulder at 939 (940) cm^{-1} is related to the non-bridging oxygen bonds of Si-O-Ca. Moreover the above bands, the peaks posited at 560 and 606 cm^{-1} could be assigned to the bending P-O vibrations, corresponding to the crystalline phosphates. The vibration at 1620 cm^{-1}

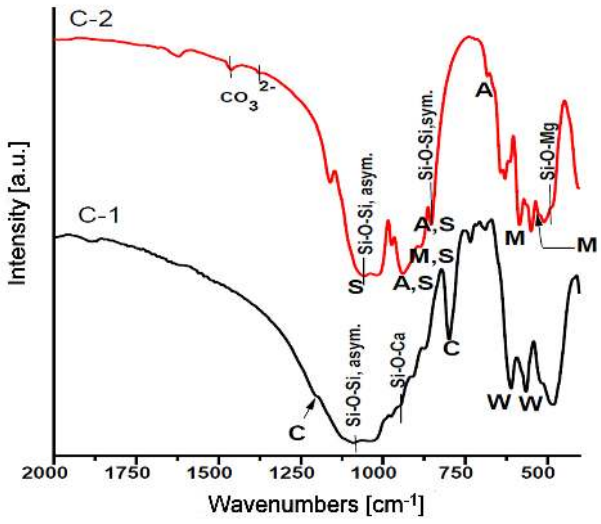

Figure 2. FTIR of the C-1 and C-2 samples thermally treated at 1200 °C for 2 h (W - whitlockite, C - cristobalite, A - akermanite, M - merwinite and S - silicocarnotite)

due to the deformation mode of H-O-H can also be observed.

The absorption bands at 560 and 606 cm^{-1}, observed in FTIR spectra of the sample C-1, could be ascribed to the $(Ca,Mg)_3(PO_4)_2$ (W) [25], and those at 795 and 1202 cm^{-1} to cristobalite (C) [22]. In addition, FTIR spectra of the sample C-2 characterize the bands posited at 939, 853 and 684 cm^{-1} related to akermanite (A) [26]. The bands centered at 884, 585 and 520 cm^{-1} could be ascribed to merwinite (M) [26] and the bands posited at 939, 884, 853 and 1060 cm^{-1} could be assigned to the silicocarnotite (S) [27]. Furthermore, the observed bands with very small intensity at 1461 and 1375 cm^{-1} can be seen in Fig. 3. The assignments for CO_3^{2-} in the prepared C-2 glass-ceramic powder are ν_3 (asymmetric stretching) at 1461 cm^{-1} and ν_2 (bending) at 1375 cm^{-1} [28]. The presence of these carbonate bands is attributed to a carbonation process of the glass-ceramic due to the

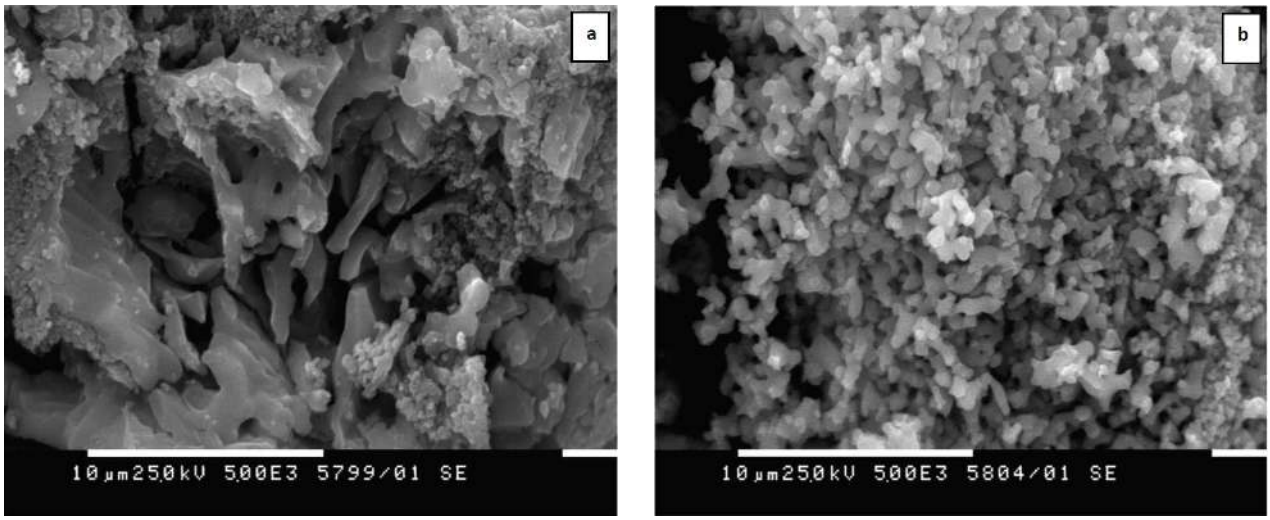

Figure 3. SEM of the C-1 (a) and C-2 (b) samples after annealing at 1200 °C for 2 hours

atmospheric CO_2 as a consequence of a high calcium content in the prepared C-2 sample. The obtained results are in a good agreement with literature data [29] for CaO-SiO_2 sol-gel glasses.

From the FTIR analysis of the thermally treated C-1 and C-2 samples we can make the following conclusions:

- the intensity of the bands at 460–600 cm^{-1} decrease with increasing of MgO content in the gels;
- the bands characteristic for cristobalite disappear with increasing of CaO and MgO content in the gels (Table 1).

Similar conclusions are valid for some biologically active glasses in SiO_2-CaO-MgO-K_2O-P_2O_5 system [30].

SEM images of the C-1 and C-2 glass-ceramics, thermally treated at 1200°C are given in Fig. 3 indicating that two samples have different morphologies, depending on the chemical compositions of the starting gels. The surface of the sample C-1 is not compact. It can be seen (Fig. 3a) that the heterogeneous surface consists of random-sized particles with sharp edges and voids among them. The pseudo prismatic and plate-like crystals could be related to cristobalite [31]. The surface of the sample C-2 consists of very small spherical particles with size of 0.3–0.5 µm and aggregated structures. In accordance with FTIR results (Fig. 2) we can conclude that these small spherical particles were formed due to the partial carbonation of the thermally treated C-2 sample.

3.2. Samples after soaking in TRIS-HCl solution

XRD of the samples soaked in TRIS-HCl buffer solution for 14 days in static conditions are given in Fig. 4. From the presented XRD results it could be seen that two new phases are present in the soaked samples: carbonate apatite, $Ca_{10}(PO_4)_6(CO_3)\times0.5(OH)$ (PDF card 01-072-7532) and hydromagnezite, $Mg_5(CO_3)_4(OH)_2\times4\,H_2O$ (PDF card 25-0513). In the sample C-1 with molar ratio Ca+Mg/Si+P = 1 (Fig. 4a) $(Ca,Mg)_3(PO_4)_2$ and SiO_2 with low crystallinity were also detected. On the other hand, the sample C-2 with molar ratio Ca+Mg/Si+P = 2.18 (Fig. 4b) does not have $Ca_2MgSi_2O_7$ and $Ca_3Mg(SiO_4)_2$ phases, i.e. these two crystalline phases were dissolved in TRIS-HCl buffer solution. The product of a particular dissolution of $(Ca,Mg)_3(PO_4)_2$, $Ca_2MgSi_2O_7$, and $Ca_3Mg(SiO_4)_2$ is $Mg_5(CO_3)_4(OH)_2\times4\,H_2O$.

The main conclusions from the presented XRD data can be summarized as follows:

- $(Ca,Mg)_3(PO_4)_2$ and SiO_2 undergo partial dissolution in TRIS-HCl buffer;
- $Ca_2MgSi_2O_7$ and $Ca_3Mg(SiO_4)_2$ are fluently dissolute in TRIS-HCl medium;
- $Mg_5(CO_3)_4(OH)_2\times4\,H_2O$ is observed as a dissolution product in both soaked samples.

Changes in the glass-surface as a function of immersion time were assessed by FTIR. Figure 5 presents FTIR data of the glass-ceramics samples, after soaking in TRIS-HCl buffer for 14 days. The FTIR spectra of the samples (Fig. 5) exhibit a decrease in intensity of the band at 930 cm^{-1}, thus, revealing a decrease in the concentration of Si-O-, i.e. SiO_4 units [32]. The presence of shoulder peak at ~960 cm^{-1} for the sample C-1 (Fig. 5a) may be attributed to C-O vibration modes in CO_3^{2-} and P-O-P bonding [33]. He *et al.* [34] related this bond to the ν_1 PO_4^{3-} vibration mode for the crystalline phosphates for the samples soaked in SBF solution. This band, together with the appearance of one with very small intensity at 894 cm^{-1}, indicates on the vibration of P-O bond [32]. In the FTIR spectrum of the sample C-1 (Fig. 5a), we cannot observe the presence of a band, posited at 1202 cm^{-1} (Fig. 2) which could be assigned to SiO_2. Moreover, the intensity of the bands at 795, 606 and 560 cm^{-1} which are characteristic for SiO_2 and $(Ca,Mg)_3(PO_4)_2$ slightly decreases. This fact could be related to the partial dissolution of these phases in TRIS-HCl buffer.

In FTIR spectrum of the sample C-1 with molar ratio Ca+Mg/Si+P = 1 (Fig. 5a) some new bands can be observed at 654, 718, 853, 1009, 1024, and

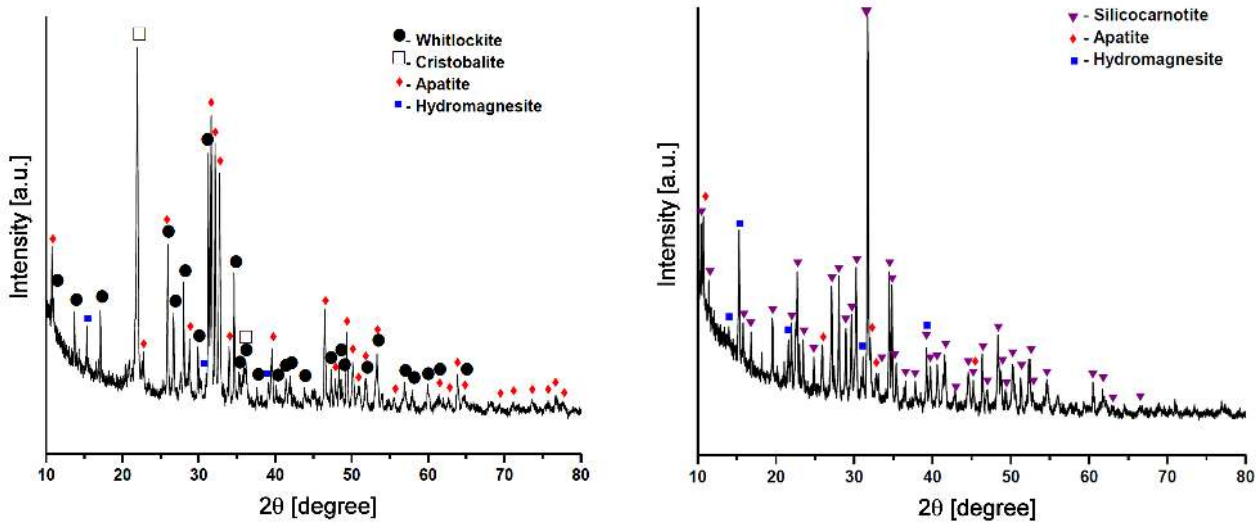

Figure 4. XRD of C-1 (a) and C-2 (b) samples after soaking in TRIS-HCl buffer for 14 days in static conditions

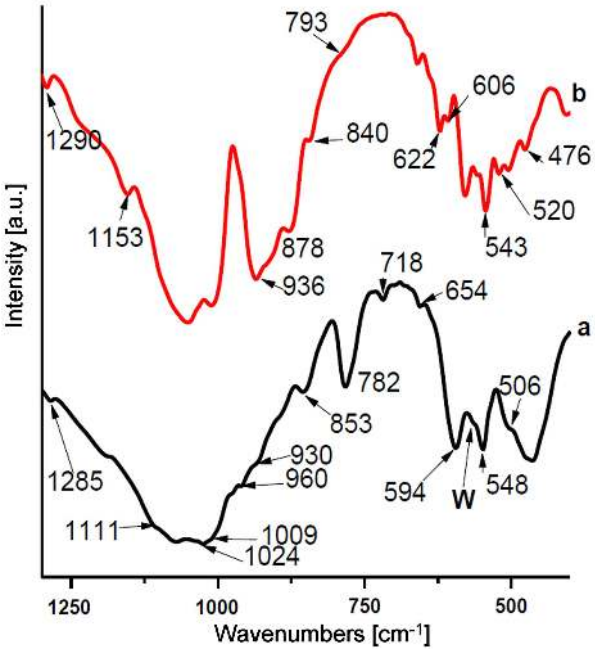

Figure 5. FTIR spectra of the glass-ceramics C-1 (a) and C-2 (b) soaked for 14 days in TRIS-HCl solution

1111 cm^{-1}. The peak posited at 654 cm^{-1} could be ascribed to the ν_4 PO_4^{3-} vibrational mode [35]. The band at 718 cm^{-1} could be determined as CO_3^{2-} in B-type CO_3HA in which $CO_3^{2-} \longrightarrow PO_4^{3-}$ [36], calcite [35], or a combination of HCO_3^- and CO_3^{2-} present in $Mg_5(CO_3)_4(OH)_2{\times}4\,H_2O$ [37]. Some research groups [38–40] proved that the peak posited at 853 cm^{-1} may be assigned to the labile CO_3^{2-} in A/B sites in CO_3HA. The peak at 1009 cm^{-1} could be related to the ν_3 PO_4^{3-} vibrational mode [36], and the others at 1024 and 1111 cm^{-1} are assigned also to the ν_3 PO_4^{3-} vibrational mode in A-type CO_3HA in which $CO_3^{2-} \longrightarrow OH^-$ [36,41]. On the other hand, the peaks posited at 594 and 853 cm^{-1} could be related to CO_3^{2-} in $Mg_5(CO_3)_4(OH)_2{\times}4\,H_2O$ [42].

From the presented FTIR results we can conclude that after immersion in TRIS-HCl buffer for 7 days, the characteristic bands for cristobalite (C) and $(Ca,Mg)_3(PO_4)_2$ undergo changes in their intensity: the intensity of these bands decrease with increasing of the soaking time. Moreover, the characteristic bands for A/B CO_3HA and $Mg_5(CO_3)_4(OH)_2{\times}4\,H_2O$ are also present.

In addition, in FTIR spectrum of the sample C-2 with molar ratio Ca+Mg/Si+P = 2.18 (Fig. 5b) the characteristic bands for akermanite (A) and merwinite (M) can not be observed, after the dissolution test in TRIS-HCl buffer for 14 days. Moreover, in the presented spectrum we can see the presence of some new bands at 520, 543 and 606 cm^{-1}. These bands could be related to ν_4 PO_4^{3-} [43,44]. The peak with low intensity, posited at 840 cm^{-1} could be related to CO_3^{2-} ion, incorporated into HA lattice in accordance with Regnier *et al.* [45]. In coincidence with some preliminary data, the peak at 878 cm^{-1} could be attributed to CO_3^{2-} in B-type CO_3HA [40]. This band and the one at 793 cm^{-1} could be related also to the $Mg_5(CO_3)_4(OH)_2{\times}4\,H_2O$ [42,46].

On the basis of the obtained results we can conclude that when the sample C-2 soaked in TRIS-HCl buffer for 14 days, the characteristic peaks for akermanite (A) and merwinite (M) could not be observed in the FTIR spectrum (Fig. 5b). On the other hand, some new peaks can be detected. The presence of these peaks could be related to the formation of new crystalline phases on the surface of the soaked samples in accordance with XRD results (Fig. 4b).

More detailed information about the structural changes caused by immersion of the samples C-1 and C-2 in TRIS-HCl buffer for 14 days are given in Fig. 6. From the presented FTIR spectra (Fig. 6) it can be

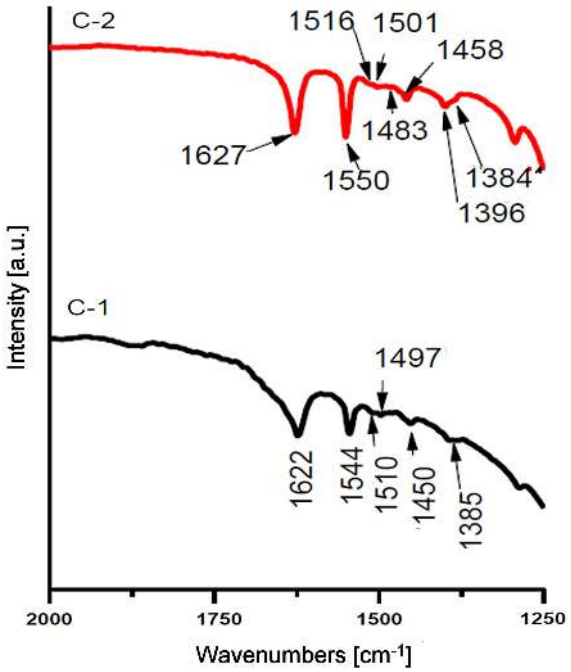

Figure 6. FTIR spectra of the soaked for 14 days in TRIS solution C-1 and C-2 glass-ceramics in the range 2000–1250 cm^{-1}

seen that the bands, centered at 1385 and 1450 cm^{-1}, for the sample C-1 could be ascribed to the presence of B-type CO_3HA, i.e. part of PO_4^{3-} was replaced by CO_3^{2-} [47,48]. The same type of substitution for the sample C-2 could be denoted by the presence of some peaks, centered at 1400, 1458, and 1483 cm^{-1} [28,48,49]. In accordance with other preliminary data the peaks, posited at 1497, 1510, and 1544 cm^{-1} for the sample C-1 and those at 1501 and 1516 cm^{-1} could be related to A-type CO_3HA in which OH^- ions are replaced by CO_3^{2-} [48,50–52]. The peak at 1550 cm^{-1} for the sample C-2 is assigned to A/B-type CO_3HA [53].

SEM images of the samples C-1 and C-2 soaked in TRIS-HCl buffer for 14 days are given in Fig. 7. From the SEM images it could be seen that the surfaces of the immersed C-1 and C-2 samples are fully covered by a new layer with particles of different morphology. The presence of these particles is related to CO_3HA, which is formed on the immersed samples in accordance with XRD (Fig. 4) and FTIR (Figs. 5 and 6) results. Moreover, in the presented SEM results we can also see the particles with plate-like morphology. These particles could be related to $Mg_5(CO_3)_4(OH)_2{\times}4\,H_2O$ [54].

XPS investigations were performed to identify chemical states and surface structures of the prepared glass-ceramics in soaked TRIS buffer for 14 days in static conditions. A survey scan XPS spectra of the immersed samples are presented in Fig. 8 and the peak positions are listed in Table 2. Furthermore, the narrow scan XPS measurements of the samples are shown in Fig. 9. The C1s peak position due to adventitious carbon was detected at the binding energy value 285.0 eV, but the C1s spectrum (Fig. 9a) shows two overlapping peaks. They could have arisen from the presence of two different chemical identities. The peaks posited at 285.0 eV for both samples could be related to the C-O bond [17]. The peaks centered at 286.9 eV (for the sample C-1) and 286.7 eV (for the sample C-2) could be ascribed to the C=O bonds [17]. These C-O and C=O bonds can be related to the surface carbonate complexes, as described in [17]. In our case, it is evident that the part of carbonate content is not incorporated into CO_3HA lattice. In the Ca2p spectrum the peak at 347.9 eV can be observed for the sample C-1. In accordance with Ni *et al.* [55] and Obst *et al.* [56] this peak could be ascribed to the small amount of aragonite. Moreover, the two peaks, centered at 347.0 eV for the samples C1 and C2 (Fig. 9b) could be assigned to the $Ca2p_{3/2}$ in HA lattice [57]. The peak at 348.5 eV for the sample C-2 could be related to $Ca2p_{3/2}$ in hydroxyapatite (HA) [56].

The observed P2p photoelectron spectrum (Fig. 9c) depicts the presence of three peaks, centered at 134.0 eV (for the sample C-1) and 134.2 and 135.1 eV (for the sample C-2). The first two peaks correspond to P2p in B-type CO_3HA [58] and PO_4^{3-} in accordance with Ad-

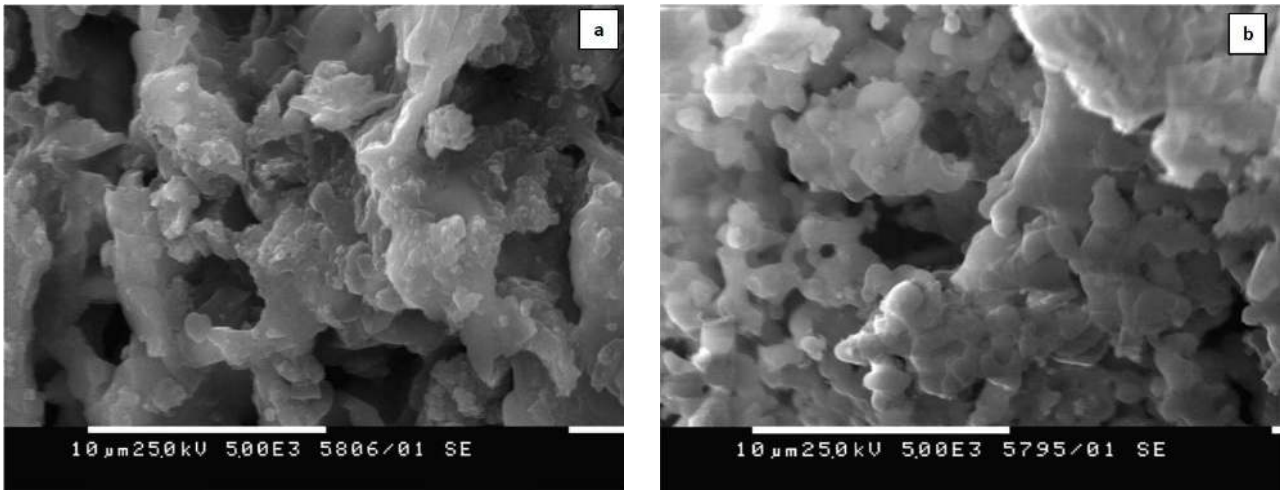

Figure 7. SEM of the C-1 (a) and C-2 (b) samples soaked in TRIS-HCl buffer for 14 days

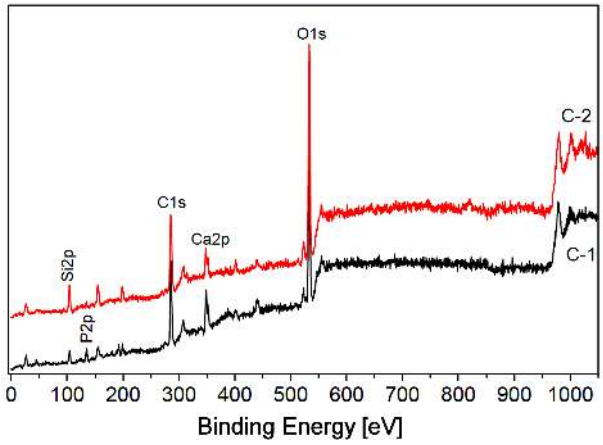

Figure 8. XPS spectra of survey scans for C-1 and C-2 glass-ceramics soaked in TRIS-HCl buffer for 14 days

min *et al.* [59]. The O1s spectrum (Fig. 9d) indicates two environments having two peaks with BE values at 532.0 eV (for both samples) and at 533.5 (532.5) eV for the samples C-1 and C-2. The first one may correspond to P-OH bonds of HA [60]. The component at 533.5 eV may be related to OH groups, and the peak at 532.5 eV is indicative for the presence of SiO_2 in which O atoms are covalently bonded to two SiO_4 tetrahedra [17]. The Si2p spectra is located at 103.5 (102.4) eV for the sample C-1, and 104.4 eV (for both samples) as can be seen from Fig. 9e. The peak at 102.4 eV could be related to Si-O- bonds [17,61], and the one at 103.5 eV to SiO_2 bulk structures [17]. Furthermore, the two peaks located at 104.4 eV could be ascribed to the silicon containing amorphous calcium phosphate (Si-ACP) [62].

Figure 10 presents ICP-AES data for the evaluation of the ionic concentration of Ca, Si, P, and Mg in the TRIS-HCl solution, after soaking of the prepared glass-ceramics for 14 days in static conditions. The Ca release rate for two glass-ceramics show a very different behavior. For the sample C-1 Ca content reaches a maximum of 447 mg/l. For this sample, P content is 5 mg/l. In accordance with [63], the low P concentration is probably the limiting factor for the growth of the CO_3HA layer, formed on the surface of the soaked samples. The lower Mg content (19 mg/l) could be related to the lower crystallinity of $Mg_5(CO_3)_4(OH)_2{\times}4\,H_2O$. The obtained ICP-AES results are in a good agreement with presented XRD data (Fig. 4a). For the glass-ceramic C-2, ICP-AES depicts that the Ca content is 147 mg/l, accompanied with low P content (7 mg/l). In accordance with XRD results (Fig. 4b), the produced CO_3HA has low crystallinity. Moreover, the sample C-2 releases high Mg content (534 mg/l) after soaking in TRIS-HCl buffer. The highest Mg content can be explained by the complete dissolution of $Ca_2MgSi_2O_7$ and $Ca_3Mg(SiO_4)_2$.

IV. Conclusions

Two novel glass-ceramics in CaO-SiO_2-P_2O_5-MgO system were synthesized via polystep sol-gel method. After thermal treatment of the dried gels at 1200 °C for 2 hours XRD proved the presence of whitlockite and cristobalite in the sample with molar ratio Ca+Mg/Si+P = 1, and silicocarnotite, akermanite, and merwinitein the sample with molar ratio Ca+Mg/Si+P = 2.18. FTIR

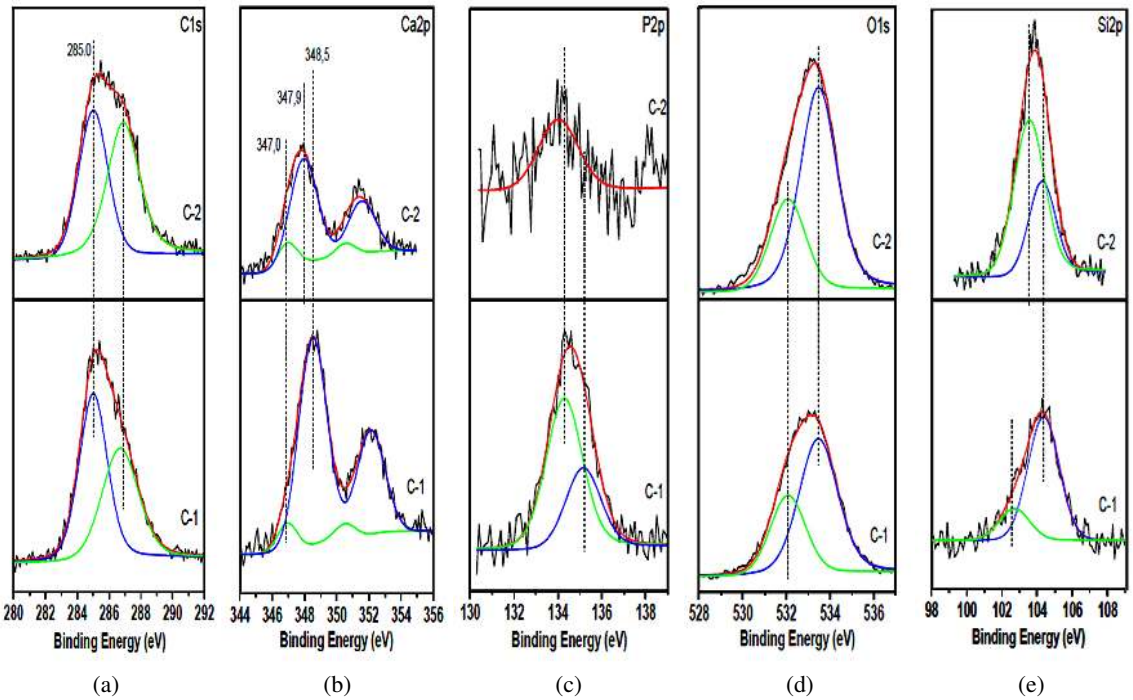

Figure 9. XPS spectra of narrow scans for immersed C-1 and C-2 glass-ceramics in TRIS-HCl buffer for 14 days in static conditions: a) C1s, b) Ca2p, c) P2p, d) O1s and e) Si2p

Table 2. Quantified XPS results for C-1 and C-2 glass-ceramics, after soaking in TRIS buffer for 14 days

Binding energy (BE) [eV]									
C1s		Ca2p		P2p		O1s		Si2p	
C-1	C-2	C-1	C-2	C-1	C-2	C-1	C-2	C-1	C-2
285.0	285.0	347.0	347.0	134.0	134.2	532.0	532.0	103.5	102.4
286.9	286.7	347.9	348.5		135.1	533.5	532.5	104.4	104.4

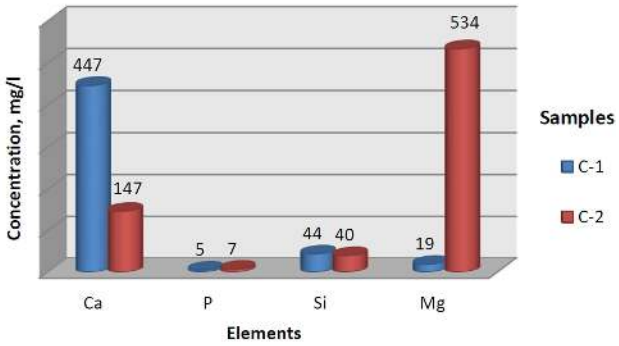

Figure 10. ACP-AES for C-1 and C-2 glass-ceramics after exposure in TRIS-HCl buffer for 14 days in static conditions

of the prepared samples showed the presence of basic absorption bands, corresponding to the different chemical bonds and crystalline phases in agreement with XRD data. SEM depicted the presence of heterogeneous surface consisted of irregular particles with different morphology depending on the compositions of the gels for the two prepared glass-ceramics.

After immersion of the studied glass-ceramics in TRIS-HCl buffer solution for 14 days in static conditions, XRD could not detect the presence of akermanite and merwinite phases. On the other hand whitlockite and cristobalite were partially dissolved in the buffer media. FTIR data are in accordance with XRD analysis. Furthermore, FTIR revealed the presence of some CO_3^{2-} bands, i.e. after soaking carbonate apatite (CO_3HA) may be formed on the surface of the prepared glass-ceramics. On the basis of FTIR results we can assume the A-type and B-type CO_3HA formed on the surface. SEM images of these samples showed that the surface of the soaked samples was fully covered with the carbonate apatite layer with different morphology. XPS analysis proved the presence of C1s, Ca2p, P2p and Si2p bonds, i.e. silicon containing carbonate apatite (Si-CO_3HA) could be formed on the surface of the prepared glass-ceramics after soaking in TRIS-HCl buffer solution.

References

1. M. Vallet-Regí, A. Salinas, J. Ramírez-Castellanos, J.M. González-Calbet, "Nanostructure of bioactive sol-gel glasses and organic-inorganic hybrids", *Chem. Mater.*, **17** [7] (2005) 1874–1879.
2. L.L. Hench, "The story of Bioglass", *J. Mater. Sci. Mater. Med.*, **17** (2006) 967–978.
3. S. Nakajima, Y. Harada, Y. Kurihara Y. Wakatsuki, H. Noma, "Physicochemical characteristics of new reinforcement ceramic implant", *Shikwa Gakuho*, **89** (1989) 1709–1717.
4. S. Nakajima, "Experimental studies of healing process on reinforcement ceramic implantation in rabbit mandible", *Shikawa Gakuho*, **90** (1990) 525–553.
5. J.-J. Shyu, J.-M. Wu, "Effects of composition changes on the crystallization behavior of MgO-CaO-SiO_2-P_2O_5 glass-ceramics", *J. Am. Ceram. Soc.*, **74** [9] (1991) 2123–2130.
6. C.T. Wu, J. Chang, N. Siyu, J. Wang, "*In vitro* bioactivity of akermanite ceramics", *J. Biomed. Mater. Res.*, **76 A** (2006) 73–80.
7. C.T. Wu, J. Chang, J.Y. Wang, S.Y. Ni., W.Y. Zhai, "Preparation and characteristics of a calcium magnesium silicate (bredigite) bioactive ceramic", *Biomaterials*, **26** [16] (2005) 2925–2931.
8. C. Wu, J. Chang, "Degradation, bioactivity, and cytocompatibility of diopside, akermanite, and bredigite ceramics", *J. Biomed. Mater. Res.: Appl. Biomater. B*, **83** (2007) 153–160.
9. C.T. Wu, J. Chang, W.T. Zhai, S.Y. Ni, J.Y. Wang, "Porous akermanite scaffolds for bone tissue engineering: Preparation, characterization, and *in vitro* studies", *J. Biomed. Mater. Res.: Appl. Biomater. B*, **78** [1] (2006) 47–55.
10. J. Ma, C.Z. Chen, D.G. Wang, J.H. Hu, "Synthesis, characterization and *in vitro* bioactivity of magnesium-doped sol-gel glass and glass-ceramics", *Ceram. Int.*, **37** [5] (2011) 1637–1644.
11. E. Bernardo, J.-F. Carlotti, P.M. Dias, L. Fiocco, P. Colombo, L. Treccani, U. Hess, K. Rezwan, "Novel akermanite-based bioceramics from preceramic polymers and oxide fillers", *Ceram. Int.*, **40** (2014) 1029–1035.
12. C.P. Yoganand, V. Selvarajan, L. Lusvarghi, O.M. Goudouri, K.M. Paraskevopoulos, M. Roubhia, "Bioactivity of CaO-MgO-SiO_2 glass ceramics synthesized using transferred arc plasma (TAP) process", *Mater. Sci. Eng. C*, **29** (2009) 1759–1764.
13. M. Hafez-Ardakani, F. Moztarzadeh, M. Rabiee, A.R. Talebi, "Synthesis and characterization of nanocrystalline merwinite ($Ca_3Mg(SiO_4)_2$) via sol-gel method", *Ceram. Int.*, **37** (2011) 175–180.
14. A. Balamurugan, G. Balossier, J. Michel, S. Kannan, H. Benhayone, A.H.S. Robelo, J.M.F. Ferreira, "Sol gel derived SiO_2-CaO-MgO-P_2O_5 bioglass system–Preparation and *in vitro* characterization", *J. Biomed. Mater. Res.: Appl. Biomater. B*, **83** (2007) 546–553.
15. D.U. Tulyaganov, S. Agathopoulos, J.M. Ventura, M.A. Karakassides, O. Fabrichinaya, J.M.F. Ferreira, "Synthesis of glass-ceramics in the CaO-MgO-SiO_2

system with B_2O_3, P_2O_5, Na_2O and CaF_2 additives", *J. Eur. Ceram. Soc.*, **26** (2006) 1463–1471.
16. D.U. Tulyaganov, S. Agathopoulos, P. Valério, A. Balamurugan, A. Saranti, M.A. Karakassides, J.M.F. Fereira, "Synthesis, bioactivity and preliminary biocompatibility studies of glasses in the system CaO-MgO-SiO_2-Na_2O-P_2O_5-CaF_2", *J. Mater. Sci: Mater. Med.*, **22** (2011) 217–227.
17. M. Cerruti, C. Bianchi, F. Bonino, A. Damin, A. Perardi, C. Morterra, "Surface modifications of bioglass immersed in TRIS-buffered solution. A multitechnical spectroscopic study", *J. Phys. Chem. B*, **109** (2005) 14496–14505.
18. L. Radev, V. Hristov, I. Michailova, B. Samuneva, "Sol-gel bioactive glass-ceramics Part I: Calcium phosphate silicate/wollastonite glass-ceramics", *Cent. Eur. J. Chem.*, **7** [3] (2009) 317–321.
19. J. Ma, C.Z. Chen, D.G. Wang, J.H. Hu, "Effect of magnesia on structure, degradability and *in vitro* bioactivity of CaO-MgO-P_2O_5-SiO_2 system ceramics", *Mater. Lett.*, **65** [1] (2011) 130–133.
20. J. Ma, C.Z. Chen, D.G. Wang, X. Shao, D.G. Wang, H.M. Zhang, "Effect of MgO addition on the crystallization and *in vitro* bioactivity of glass ceramics in the CaO-MgO-SiO_2-P_2O_5 system", *Ceram. Int.*, **38** (2012) 6677–6684.
21. S.J. Watts, R.G. Hill, M.D. O'Donnell, R.V. Law, "Influence of magnesia on the structure and properties of bioactive glasses", *J. Non-Cryst. Solids*, **356** (2010) 517–524.
22. E. Dowty, "Vibrational interactions of tetrahedra in silicate glasses and crystals II. Calculations on melities, pyroxenes, silica polymorphs and feldspars", *Phys. Chem. Minerals*, **14** (1987) 122–138.
23. J. Ma, C.Z. Chen, D.G. Wang, X.G. Meng, J.Z. Shi, "Influence of the sintering temperature on the structural feature and bioactivity of sol-gel derived SiO_2-CaO-P_2O_5 bioglass", *Ceram. Int.*, **36** (2010) 1911–1916.
24. B. Samuneva, S. Kalimanova, E. Kashchieva, P. Djambaski, I.M.M. Salvado, M.H. Fernandes, "Composite glass-ceramics in the systems MgO-SiO_2, MgO-Al_2O_3-SiO_2 and fluorapatite obtained by sol-gel technology", *J. Sol-Gel Sci. Technol.*, **26** (2003) 273–278.
25. H. Li, A. Ito, Y. Sogo, X. Wang, R.Z. Le Geros, "Solubility of Mg-containing β-tricalcium phosphate at 25 °C", *Acta Biomater.*, **5** [1] (2009) 508–517.
26. O.M. Goudouri, E. Theodosoglou, E. Kontonasaki, J. Will, K. Chrissafis, P. Kiodis, K.M. Paraskevopoulos, A.R. Boccaccini, "Development of highly porous scaffolds based on bioactive silicates for dental tissue engineering", *Mater. Res. Bull.*, **49** (2014) 399–404.
27. S. Serena, M.A. Sainz, A. Caballero, "Single-phase silicocarnotite synthesis in the subsystem $Ca_3(PO_4)_2$-Ca_2SiO_4", *Ceram Int.*, **40** (2014) 8245–1852.
28. L. Radev, V. Hristov, I. Michailova, M.H.V. Fernandes, I.M.M. Salvado, "*In vitro* bioactivity of biphasic calcium phosphate silicate glass-ceramicin CaO-SiO_2-P_2O_5 system", *Process. Appl. Ceram.*, **4** [1] (2010) 15–24.
29. A. Martinez, I. Izquierdo-Barba, M. Vallet-Regi, "Bioactivity of a CaO-SiO_2 binary glasses system", *Chem. Mater.*, **12** (2000) 3080–3088.
30. M. Szumera, I. Waklawska, W. Mozgawa, M. Sitarz, "Spectroscopic study of biologically active glasses", *J. Mol. Struct.*, **744-747** (2005) 609–614.
31. C.J. Horwell, B.J. Williamson, E.W. Llewellin, D.E. Damby, J.S. Le Blond, "The nature and formation of cristobalite at the Soufrière Hills volcano, Montserrat: implications for the petrology and stability of silicic lava domes", *Bull. Volcanol.*,**75** (2013) 696–715.
32. J. Massera, L. Hupa, M. Hupa, "Influence of the partial substitution of CaO with MgO on the thermal properties and *in vitro* reactivity of the bioactive glass S53P4", *J. Non-Cryst. Solids*, **358** (2012) 2701–2707.
33. I. Rehman, J.C. Knowles, W. Bonfield, "Analysis of in vitro reaction layers formed on bioglass using thin-film X-ray diffraction and ATR-FTIR microspectroscopy", *J. Biomed. Res.*, **41** (1998) 162–166.
34. Q. He, Z. Huang, Y. Liu, W. Chen, T. Xu, "Template-directed one-step synthesis of flowerlike porous carbonated hydroxyapatite spheres", *Mater. Lett.*, **61** [1] (2007) 141–143.
35. H.E. Feki, C. Rey, M. Vignoles, "Carbonate ions in apatites: infrared investigations in the ν_4 CO_3 domain", *Calcif. Tissue. Int.*, **49** [4] (1991) 269–274.
36. G. Penel, G. Leroy, C. Rey, E. Bres, "MicroRaman spectral study of the PO_4 and CO_3 vibrational modes in synthetic and biological apatites", *Calcif. Tissue. Int.*, **63** [6] (1998) 475–481.
37. R.L. Frost, "Raman spectroscopic study of the magnesium carbonate mineral hydromagnesite ($Mg_5[(CO_3)_4(OH)_2] \cdot 4\,H_2O$)", *J. Raman Spectrosc.*, **42** (2011) 1690–1694.
38. M.E. Fleet, "Infrared spectra of carbonate apatites: ν_2-region bands", *Biomater.*, **30** [8] (2009) 1473–1481.
39. E.P. Paschalis, E. DiCarlo, F. Betts, P. Sherman, R. Mendelsohn, A.L. Boskey, "FTIR microspectroscopic analysis of human osteonal bone", *Calcif. Tissue. Int.*, **59** [6] (1996) 480–487.
40. C. Rey, V. Renugopalakrishman, B. Collins, M.J. Glimcher, "Fourier transform infrared spectroscopic study of the carbonate ions in bone mineral during aging", *Calcif. Tissue Int.*, **49** [4] (1991) 251–258.
41. D.P. Minh, N.D. Tran, A. Nzihou, P. Sharrock, "Carbonate-containing apatite (CAP) synthesis under moderate conditions starting from calcium carbonate and orthophosphoric acid", *Mater. Sci. Eng. C*, **33** [5] (2013) 2971–2980.

42. M. Jonson, D. Persson, D. Thierry, "Corrosion product formation during NaCl induced atmospheric corrosion of magnesium alloy AZ91D", *Corrosion Sci.*, **49** (2007) 1540–1558.
43. S. Dorozhkin, "In vitro mineralization of silicon containing calcium phosphate bioceramics", *J. Am. Ceram. Soc.*, **90** [1] (2007) 244–249.
44. J.C. Elliott, D.W. Holcomb, R.A. Young, "Infrared determination of the degree of substitution of hydroxyl by carbonate ions in human dental enamel", *Calcif. Tissue. Int.*, **37** [4] (1985) 372–375.
45. P. Regnier, A.C. Lasaga, R.A. Berner, O.H. Han, K.W. Zilm, "Mechanism of CO_3^{2-} substitution in carbonate-fluorapatite; evidence from FTIR spectroscopy, ^{13}C NMR, and quantum mechanical calculations", *Amer. Mineral.*, **79** (1994) 809–818.
46. A. Botha, C.A. Strydom,"DTA and FT-IR analysis of the rehydration of basic magnesium carbonate", *J. Thermal. Anal. Calorim.*, **71** (2003) 987–995.
47. D.S. Tavares, C.H. Resende, M.P. Quitan, L.O. Castro, J.M. Granjeiro, G.A. Soares, "Incorporation of strontium up to 5 mol.% to hydroxyapatite did not affect its cytocompatibility", *Mater. Res.*, **14** [4] (2011) 456–460.
48. C. Rey, B. Collins, T. Goehl, I.R. Dickson, M.J. Glimcher, "The carbonate environment in bone mineral: A resolution-enhanced Fourier Transform Infrared Spectroscopy Study", *Calcif. Tissue Int.*, **45** [3] (1989) 157–164.
49. Y. Yusufoglu, M. Akinc, "Effect of pH on the carbonate incorporation into the hydroxyapatite, prepared by an oxidative decomposition of calcium EDTA chelate", *J. Am. Ceram. Soc.*, **91** [1] (2008) 77–82.
50. J.P. Lafon, E. Champion, D. Bernache-Assollant, R. Gibert, A.M. Danna, "Termal decomposition of carbonated calcium phosphate apatites", *J. Thermal. Anal. Calorim.*, **72** [3] (2003) 1127–1134.
51. I. Hofmann, L. Müller, P. Greil, F.A. Müller, "Precipitation of carbonated calcium phosphate powdersfrom a highly supersaturated simulated body fluidsolution", *J. Am. Ceram. Soc.*, **90** [3] (2007) 821–824.
52. M.E. Fleet, X. Liu, P.L. King, "Accommodation of the carbonate ion in apatite: An FTIR and X-ray structure study of crystals synthesized at 2–4 GPa", *Amer. Mineral.*, **89** (2004) 1422–1432.
53. L. Radev, T. Gerganov, H. Georgiev, A. Kolev, V. Vassileva, R. Iankova, E. Cholakova, "Silk fibroin/calcium phosphate silicate composites: *In vitro* bioactivity", *Int. J. Mater. Chem.*, **3** [3A] (2013) 8–15.
54. I.M. Power, S.A. Wilson, J.M. Thom, G.D. Dipple, J.E. Gabites, G. Southam, "The hydromagnesite playas of Atlin, British Columbia, Canada: A biogeochemical model for CO_2 sequestration", *Chem. Geol.*, **260** (2009) 286–300.
55. M. Ni, B.D. Ratner, "Differentiating calcium carbonate polymorphs by surface analysis techniques – an XPS and TOF-SIMS study", *Surf. Interface Anal.*, **40** [10] (2008) 1356–1361.
56. M. Obst, J.J. Dynes, J.R. Lawrence, G.D.W. Swerhone, K. Benzerara, C. Karunakaran, K. Kaznatcheev, T. Tyliszczak, A.P. Hitchcock, "Precipitation of amorphous $CaCO_3$ (aragonite-like) by cyanobacteria: A STXM study of the influence of EPS on the nucleation process", *Geochim. Cosmochim. Acta*, **73** (2009) 4180–4198.
57. R.-J. Chung, M.-F. Hsieh, R.N. Panda, T.-S. Chin, "Hydroxyapatite layers deposited from aqueous solutions on hydrophilic silicon substrate", *Surf. Coat. Techn.*, **165** (2003) 194–200.
58. R. França, T.D. Samani, G. Bayade, L.H. Yahia, E. Sacher, "Nanoscale surface characterization of biphasic calcium phosphate, with comparisons to calcium hydroxyapatite and β-tricalcium phosphate bioceramics", *J. Colloid Interface Sci.*, **420** (2014) 182–188.
59. M.S. Amin, L.K. Randeniya, A. Bendavid, P.J. Martin, E.W. Preston, "Biomimetic apatite growth from simulated body fluid on various oxide containing DLC thin films", *Diamond Related Mater.*, **21** (2012) 42–49.
60. X. Zhao, T. Hu, H. Li, M. Chen, Sh. Cao, L. Zhang, X. Hou, "Electrochemically assisted codeposition of calcium phosphate/collagen coatings on carbon/carbon composites", *Appl. Surf. Sci.*, **257** (2011) 3612–3619.
61. Z. Leilei, L. Hejun, L. Kezhi, F. Qiangang, Zh. Yulei, L. Shoujie, "A Na and Si co-substituted carbonated hydroxyapatite coating for carbon nanotubes coated carbon/carbon composites", *Ceram. Int.*, **40** (2014) 13123–13130.
62. C. Chow, C.D. Wu, C.A. Evans, "In vitro properties of orthodontic adhesives with fluoride or amorphous calcium phosphate", *Int. J. Dent.*, **2011** (2011) 1–8.
63. M.M. Pereira, A.E. Clark, L.L. Hench, "Calcium phosphate formation on sol-gel-derived bioactive glasses in vitro", *J. Biomed. Mater Res.*, **28** (1994) 693–698.